

Science

Prediction of the structure of the martian upper atmosphere for the Mars Reconnaissance Orbiter (MRO) mission

Stephen W. Bougher¹, James R. Murphy², Jared M. Bell¹, and Richard W. Zurek³

¹Atmospheric, Oceanic, and Space Sciences Department, University of Michigan, Ann Arbor, MI, 48109, USA, bougher@umich.edu; ²Dept. of Astronomy, New Mexico State University, Las Cruces, NM, 88003, USA; ³Jet Propulsion Laboratory, California Institute of Technology, Pasadena, CA, 91109, USA

Citation: Mars 2, 10-20, 2006; [doi:10.1555/mars.2006.0002](https://doi.org/10.1555/mars.2006.0002)

History: Submitted: April 3, 2006; Reviewed: April 28, 2006; Revised: May 26, 2006; Accepted: May 30, 2006; Published: June 16, 2006

Editor: François Forget, Institut Pierre Simon Laplace, Laboratoire de Météorologie Dynamique

Reviewers: John Wilson, Geophysical Fluid Dynamics Laboratory, National Oceanic and Atmospheric Administration; Paul Withers, Center for Space Physics, Boston University

Open Access: Copyright © 2006 Bougher et al. This is an open-access paper distributed under the terms of a [Creative Commons Attribution License](https://creativecommons.org/licenses/by/4.0/), which permits unrestricted use, distribution, and reproduction in any medium, provided the original work is properly cited.

Abstract

Background: The Mars Reconnaissance Orbiter (MRO) spacecraft was launched toward Mars from the Kennedy Space Center in Florida on August 12, 2005, and arrived at Mars on March 10, 2006. Aerobraking in the Martian lower thermosphere (~100-200 km) is planned for 6-months after arrival, enabling the desired mapping orbit to be achieved. Knowledge of the Mars upper atmosphere structure is important for ensuring a safe and successful aerobraking process.

Method: Previous Mars Global Surveyor (MGS) density data, acquired during Phase 2 (MGS2) aerobraking operations, is used to validate new coupled MGCM-MTGCM (General Circulation Model) simulations. Confidence gained from this analysis is used to make new predictions for anticipated MRO densities during its aerobraking phase. Specific Mars conditions approaching the aphelion season ($L_S \sim 30-110$) are prescribed in the MGCM-MTGCM inputs.

Conclusion: Predicted densities for MRO are simulated to decrease toward the southern winter pole, in accord with the general trend observed during MGS2. However, it is clear that MRO predicted densities at 120 km are smaller than observed MGS2 densities (especially at similar latitudes near $L_S \sim 85$). The distinct solar local time sampling planned for MRO, during a different interval of the solar cycle, may contribute to these differences. The new MRO MGCM-MTGCM predictions described in this paper are being used to support MRO aerobraking activities.

Introduction

The Mars Reconnaissance Orbiter (MRO) spacecraft was launched toward Mars from the Kennedy Space Center in Florida on August 12, 2005, and arrived at Mars on March 10, 2006. After being captured into a gravitationally bound orbit around Mars, achieved via spacecraft deceleration induced by the firing of onboard engines, orbit modification via the process of aerobraking will commence and nominally continue for six months. At the conclusion of a successful aerobraking phase, the spacecraft will be in a near-circular near-polar sun synchronous orbit, which is desired for the mapping phase of the mission. The ability to anticipate the atmospheric conditions MRO will experience in the 100-200

km altitude range as it passes through Mars' upper atmosphere is an important component for successful completion of aerobraking. Previous aerobraking experience at Mars provides one indication of conditions MRO might experience. Numerical models provide an additional tool, and enable investigation of possible conditions more specific to the space and time domain for which MRO will be aerobraking

The cost of sending an orbiting spacecraft to Mars ranges from \$350-750M. Roughly 20-30% of this cost goes toward the launch costs. Prior to the 1996 launch of the Mars Global Surveyor (MGS) orbiter, launch costs included the expense of launching and sending off to Mars the fuel which spacecraft

rocket engines then employed to slow the spacecraft upon Mars arrival into a capture orbit and then to subsequently modify this capture orbit to a more appropriate science phase orbit. Beginning with MGS, reduced spacecraft launch mass has been achieved via implementation of the process of aerobraking. Aerobraking employs frictional drag between an orbiting spacecraft and the upper atmosphere of the planet (or moon) being orbited. The drag occurs when the spacecraft orbital periapsis is located at an altitude which places the spacecraft within the tenuous upper atmosphere. The reduction of the spacecraft's speed at the periapsis of its eccentric orbit due to the dynamic pressure imparted upon the spacecraft by the atmosphere reduces the orbital period and eccentricity. Repeated drag passes can ultimately lead to a near circular orbit, after which an engine burn (orbital speed increase) at orbit apoapsis raises the periapsis out of the atmosphere and circularizes the orbit. A circular (or near circular) orbit is an optimal condition for a nadir viewing sun-synchronous orbiting spacecraft. Use of this atmospheric friction to modify the initial orbit reduces the need for fuel at launch, which reduces the overall mission cost.

In order for aerobraking to be cost effective, the spacecraft must survive the aerobraking process and be placed into the desired mission mapping phase orbit. In order to achieve these dual constraints of safety and complete orbit modification, aerobraking is driven by two competing limits: too little drag (resulting from too low an atmospheric density) over successive orbits does not allow the evolving orbit to 'lock in' at the desired sub-spacecraft local time, while too large a density on any given drag pass can produce excessive dynamic heating which can damage the spacecraft. Such dynamic heating is proportional to the atmospheric density times the cube of the spacecraft velocity; the dynamic pressure, which decelerates the spacecraft, is proportional to atmospheric density times the square of the spacecraft velocity. Knowledge of the atmospheric density state is very important for ensuring a safe and successful aerobraking process.

Aerobraking has been successfully employed to produce appropriate mission science phase orbits for two spacecraft, the Mars Global Surveyor (MGS) and the Mars Odyssey (ODY) spacecraft. MGS' aerobraking phases extended from September 1997 to March 1999 and ODY's from October 2001 – January 2002 (e.g. Keating et al. 2003; Withers et al. 2003; Withers 2006). Aerobraking was first tested at Venus by the Magellan spacecraft in 1993, near the conclusion of that mission (e.g. Keating and Hsu 1993). This successful test resulted in aerobraking becoming an integral part of the subsequent MGS, ODY and MRO missions. Aerobraking was also to be a mission component of the Mars Climate Orbiter upon its Mars arrival in September 1999, but the loss of that craft upon Mars arrival precluded the aerobraking mission phase.

MGS and ODY aerobraking provided significant quantities of information regarding the atmospheric mass and thermal fields at altitudes spanning 95-200 km above the martian surface (e.g. Keating et al. 1998; 2003; Tolson et al. 1999;

2005; Withers et al. 2003; Withers 2006). MGS aerobraking periapsis passes temporally sampled early martian northern autumn ($L_S = 180$) through to the following northern summer ($L_S = 100$) at northern middle latitudes. An approximately six month hiatus in aerobraking, extending from $L_S = 300$ to $L_S = 25$, was included in this time interval. During this hiatus, periapsis latitude migrated slowly northward from northern middle latitude during northern autumn. After the hiatus, periapsis migrated southward from high northern latitudes to the south pole over the time span of northern spring (southern autumn) (see Table 1). ODY aerobraking periapsis passes (~330 orbits) were far fewer in number than for non-hiatus MGS (~800 orbits), spanning a much shorter L_S range (260-310) and a more restricted latitude range (high northern latitudes initially, passing near the pole at $L_S = 290$ and then migrating southward to 20 N at the conclusion).

Table 1. MGS Phase 2 Latitudinal Density Variations at 120 km.

L_S	Latitude	SLT (hours)	MGS2 Zonal Mean Density (kg/km ³)	MTGCM Zonal Mean Density (kg/km ³)
30-60	60N-30N	17.0	10.7	9.5
60-80	30N-30S	16.0	6.2	4.2
80-85	30S-60S	15.0	4.2	2.8
85-90	60S-90S	changing	2.8	2.6
90-95	90S-60S	2.0	2.3	1.7

¹ Density units (kg/km³) are those used in aerobraking operations. These units can be translated to kg/m³ by multiplying by 1.0×10^{-9} .

Significant spatial and temporal variations in the densities experienced by MGS and ODY have been identified and studied. Longitudinal density variations (at low-to-mid latitudes), with amplitudes up to 40% of the mean, are likely connected to the influence of so called "non-migrating" thermal tide components (consisting of eastward traveling as well as non-sun-synchronous westward traveling tides) which near sun-synchronous sampling 'sees' a stationary wave component (e.g. Forbes and Hagan 2002; Forbes et al. 2002; Wilson 2002; Bougher et al. 2004; Angelats-i-coll et al. 2004). The presence of thermal tidal components in the martian atmosphere have been clearly established from analyses and modeling of surface pressure measurements and lower-atmosphere temperatures (Wilson and Hamilton, 1996; Bridger and Murphy, 1998; Banfield et al., 2000, 2003; Wilson, 2000). Traveling waves have also been observed at high latitudes near the "polar vortex" during ODY aerobraking in the northern polar night (Tolson et al. 2005). Finally, density variations also arise due to heating of the lower atmosphere (due to a developing dust storm) resulting in 'inflation' of the lower atmosphere which increases the mean pressure at greater heights and increases densities at those same heights (ignoring any in situ aerobraking altitude temperature variations) (e.g. Keating et al. 1998; Bougher et al. 1999).

Analyses of these observations have provided some ability to

anticipate conditions that MRO might experience during its aerobraking. However, MRO's season and latitude conditions do not exactly match those of either MGS or ODY, and there is no guarantee that the atmospheric thermodynamic state that MRO will experience will be identical to that of either ODY or MGS.

The MRO aerobraking phase is scheduled to commence in early martian northern Spring ($L_S = 30$) and continue through early northern Summer ($L_S = 109$), spanning nearly 550 orbits. Periapsis latitude will migrate slowly poleward/southward from 70S latitude upon aerobraking initiation, and after a near South pole passage near $L_S = 70$, periapsis latitude will more rapidly migrate northward to northern subtropical latitudes at aerobraking conclusion. These season and latitude conditions are similar to a subset of those experienced by MGS during its post hiatus aerobraking phase (Phase 2). While MGS did provide some data that might directly relate to conditions that MRO might experience, the MGS data are not extensive enough to sufficiently characterize the range of potential MRO aerobraking conditions. One means of investigating a wider range of conditions than the MGS data provide is to employ numerical models to investigate the aerobraking-altitude response of the atmosphere to a range of in situ and remote conditions: solar EUV flux, varying dust content of the lower atmosphere, etc.

Numerical models have previously been employed to study the lower martian thermosphere (e.g. Bougher et al. 1999; 2000; 2004; 2006; [Angelats-i-coll et al. 2004](#); 2005; [Gonzalez-Galindo et al. 2005](#)). These model simulations provide global (3-D) neutral temperature, density, and wind fields above 100 km, incorporating different coupling schemes for linking the Mars lower and upper atmospheres. Global grid output fields are typically compared with available (spatially and temporally limited) datasets for the purpose of model validation. Once reasonable model validation is confirmed, predictions are made for other sampling periods and locations.

Within this paper we present a prediction of the atmospheric conditions that the Mars Reconnaissance Orbiter can anticipate during its aerobraking phase. The predicted conditions arise from numerical simulations conducted with the University of Michigan Mars Thermosphere General Circulation Model (MTGCM) 'driven' from below by the NASA Ames Mars General Circulation Model (MGCM). The coupled model system is first demonstrated to credibly mimic the thermospheric structure observed by MGS. Thereafter, model results are analyzed for the season and latitudes and heights relevant to the MRO aerobraking phase. Both mean state and perturbations (spatial and temporal) are quantified that will enable one to estimate the height of the "corridor" in which aerobraking is both effective and safe, and to assess excursions about the corridor mean which arise owing to expected atmospheric variability.

Previous MGS and ODY Datasets

Both the MGS and ODY orbiter missions have provided accelerometry-derived measurements of the structure of Mars' upper atmosphere during their aerobraking mission phases. The derived values of atmospheric density, temperature, and atmospheric scale height have shown evidence of spatial (latitude, longitude) and temporal (diurnal, seasonal, solar cycle) variations in these physical states of the upper atmosphere (e.g. Keating et al. 1998; 2003; Bougher et al. 1999a; 2000; [2006,b](#); Tolson et al. 1999; 2005; Withers et al 2003; [Withers 2006](#)).

There are also seemingly quasi-random density variations present, which could be the result of the breaking of vertically propagating waves (e.g. [Angelats-i-coll et al. 2005](#); Tolson et al. 2005). Some of the specific phenomena identified in the derived density fields include: longitudinal density wave structure (at a given geopotential altitude) likely associated with atmospheric thermal tides (Forbes and Hagan 2000; [Forbes et al. 2002](#); [Wilson 2002](#); Withers et al. 2003; [Bougher et al. 2004](#); [Angelats-i-coll et al. 2004](#)), latitude variations characterized by declining density (at a given geopotential altitude) with increasing latitude in both hemispheres (Keating et al. 2003; [Bougher et al. 2006](#); [Withers 2006](#)); hemispheric differences in the occurrence of winter-time polar warming at aerobraking altitudes (100-130 km) (Keating et al. 2003; [Bougher et al. 2006](#)) and inter-annual variations in martian thermosphere densities and temperatures owing to changing lower atmosphere conditions (e.g. dust distributions) from one Mars year to the next ([Lillis et al. 2005](#); Bougher et al. 2006b).

For this current effort, we focus upon the measurements obtained by MGS during its Phase 2 (MGS2) aerobraking period (see Keating et al. 2001a,b), since those data overlap in space (latitude) and season the atmosphere which MRO will experience during its nominal aerobraking phase (see Tables 1 and 2). This overlap is most direct near $L_S = 85-95$, when MGS experienced and MRO will experience orbit periapsis at approximately 75 and 60 degrees south.

Table 1 summarizes MGS2 120 km zonal mean density data as sorted into five latitude (and L_S) bins. Figure 1 illustrates the same MGS2 density data, providing some indication of latitude variation in the zonal mean density. However, any inferred latitudinal pattern is also influenced by seasonal changes which occur through this late southern autumn and very early southern winter season covered by these MGS2 data. Ignoring the seasonal effects for the moment, the latitude pattern exhibits a persistent decline in 120 km density extending from northern middle latitudes to the south pole. For instance, equator-to-pole mean densities decrease by a factor of 2.5-3.0 (dayside). Additionally, a dayside-to-nightside decline of 120 km density at high southern latitudes is revealed from these diurnal measurements.

Figure 1 (green curve) also indicates that MGS2 periapsis altitudes decreased as the spacecraft approached high southern latitudes, at which time the craft was chasing 'downward' the optimal density for aerobraking. That the altitude of that density surface declined as periapsis migrated

poleward is hydrostatically consistent with the poleward decline in lower atmosphere temperatures, which have the effect of ‘collapsing’ the thickness of a given atmospheric column. Such a poleward decrease in atmospheric temperature throughout the bottom few scale heights of the atmosphere was indicated by atmospheric temperatures derived from Thermal Emission Spectrometer (TES) spectra (e.g. Smith 2004).

Each of these five latitude data bins also exhibit longitudinal structure (which plays a significant role in the vertical scatter present in Figure 1). At middle northern latitudes ($L_s = 30-60$), a wave-three pattern is present, with an amplitude $\sim 25\%$ of the mean density (10.7 kg/km^3). At equatorial latitudes ($L_s = 60-80$), a weak wave-three pattern is present with an amplitude that is $\sim 15\%$ of the mean 120 km density (6.2 kg/km^3) and a longitudinal phase that is similar to that at mid-northern latitudes. At middle southern latitudes ($L_s = 80-85$), a prominent wave three pattern is also present, with an amplitude that is $\sim 30\%$ of the mean density (4.2 kg/km^3). At high southern latitudes ($L_s = 85-90$), the longitudinal density structure is dominated by a wave 2 pattern (amplitude 30% of the mean of 2.8 kg/km^3), with the maximum wave peak at 225 W (135E) longitude. The subsequent equatorward/ nightside migration of the MGS periapsis location during the $L_s = 90-95$ time interval exhibited a 120 km density characterized by a longitudinal wave 3 pattern, with a phase that is shifted slightly westward from the wave-3 phases apparent as MGS approached the pole. The periapsis solar local time was $\sim 1500 \text{ SLT}$ prior to MGS passing ‘over’ the

south pole. After pole passage, the solar local time of periapsis shifted to $\sim 0200 \text{ SLT}$ (Table 1).

Coupled MGCM-MTGCM Modeling

While the in-situ MGS and ODY accelerometer measurements do characterize Mars’ upper atmosphere at the locations, seasons, and times of day sampled, they are in no way thorough in their coverage. Thus, using their results to provide a characterization for subsequent aerobraking activities (such as the upcoming MRO aerobraking mission phase) does not necessarily provide a valid estimate of the conditions to be anticipated. Numerical modeling can provide spatial and temporal estimates of the atmospheric thermodynamic state at aerobraking altitudes, seasons, and locations, but these models must be validated against the available data.

A coupled system of a Mars upper atmosphere (thermosphere) numerical model and a Mars lower atmosphere numerical model has previously been developed and employed to investigate the MGS and ODY aerobraking data sets (e.g. Bougher et al. 2004; 2006, 2006).

The basic operation of this coupled system has been execution of a lower-atmosphere simulation (employing the NASA Ames Mars General Circulation Model (MGCM), with a model top near 85 kilometers), with the atmosphere thermally forced by the radiative energy exchange in response to imposed atmospheric dust loads. These atmospheric dust loads (spatial variations of dust optical depth) are provided by the dust optical depths derived from MGS Thermal Emission Spectrometer (TES) spectra (Liu et al. 2003; Smith 2004). Globally uniform dust optical depths can also be used reliably for near aphelion conditions. The dust’s vertical distribution is prescribed using the parameterization of Conrath (1975). Following completion of an annual or multi-annual simulation so forced, MGCM results (temperatures, geopotential heights, winds) at the 1.32 microbar pressure level for a specific season are used to provide lower boundary conditions (at 2-minute time steps, on a $5^\circ \times 5^\circ$ grid) for the Mars Thermosphere General Circulation Model (MTGCM), which spans the vertical range from $\sim 70 \text{ km}$ to 300 km altitude. This detailed coupling scheme captures both migrating and non-migrating upward propagating tides plus the thermal expansion and contraction of the Mars lower atmosphere with the passage of the seasons and dust storm events (Bougher et al. 2004; 2006). These lower boundary conditions for the MTGCM also include diurnal variations present within the MGCM, as well as spatial variations arising due to hemispheric seasonal differences. These boundary conditions are ‘one way’: the lower atmosphere forcing drives the thermosphere, but the thermosphere does not in turn affect the lower atmosphere.

Previous MGCM-MTGCM simulations have been used successfully to explain the martian lower thermosphere winter polar warmings, and their seasonal variations (aphelion and perihelion), owing to changing solar insolation and lower atmosphere dust distributions (Bougher et al.

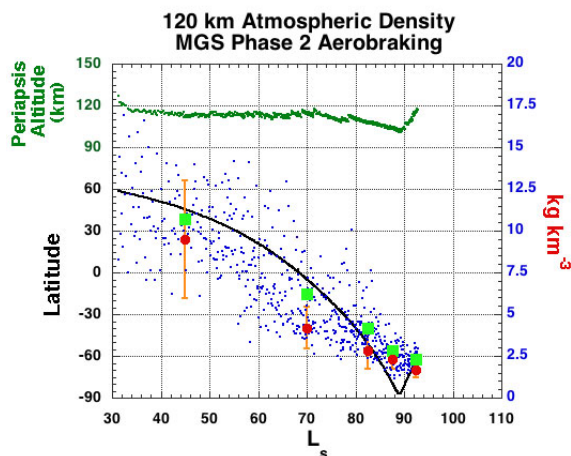


Figure 1. MGS2 aerobraking observed and modeled densities at 120 km as a function of latitude. The green curve (see PDS MGS Accelerometer archive, Keating et al. 2001a,b) tracks the MGS2 periapsis altitude variation as a function of L_s . The black curve (same MGS archive) tracks the MGS2 latitude variation. The blue dots (same MGS archive) represent individual MGS2 Accelerometer density measurements. The associated green boxes (see Table 1) represent MGS2 zonal mean densities for specific L_s periods. The red dots (mean) and associated vertical bars (longitude variation) indicate the MTGCM simulated densities (see Table 1). Density units are kg/km^3 . (figure1.jpg)

2006). These seasonal changes regulate the inter-hemispheric circulation, whose subsiding component in the winter polar region provides adiabatic heating. This heating is strong during the perihelion period for the northern winter polar region (yielding warm ODY temperatures), yet weak during the opposite aphelion period for the southern winter polar region (producing little polar warming during MGS2). In addition, MGCM-MTGCM simulated thermal tidal amplitudes in the aphelion polar dayside region (near 130 km) have been shown to drive corresponding variations in the height of the ionospheric peak, in accord with MGS Radio Science observations (Bougher et al. 2004). The ability of the coupled MGCM-MTGCM to capture high latitude upward propagating non-migrating tides during aphelion conditions is confirmed.

New MGCM-MTGCM coupled model simulations are now conducted to specifically approximate atmospheric conditions for the MGS2 aerobraking period and upcoming MRO aerobraking exercises. Inputs for the MGS2 simulations are as follows: (a) solar fluxes ($F_{10.7}=130$ index), (b) season ($L_S = 90$), and (c) dust conditions ($\tau = 0.3$, $CR = 0.3$, globally uniform distribution). CR is the Conrath parameter chosen to prescribe a shallow vertical dust distribution; τ is the integrated visible dust opacity corresponding to average aphelion conditions (Bougher et al. 2006). Inputs for the MRO simulations are as follows: (a) solar fluxes ($F_{10.7}=100$), (b) seasons ($L_S = 30,90$), and (c) dust conditions (similar to above). See Table 2 (modelinputs.txt supporting dataset) for a more comprehensive list of MGCM-MTGCM input parameters.

Analysis of MGCM-MTGCM coupled model results for these MGS2 and MRO aerobraking intervals are now presented. These new MGCM-MTGCM simulations reproduce many of the observed characteristics of the Mars structure in the 100-130 km altitude region during the MGS2 sampling period. Specifically, we compare MGS2 120 km density data with corresponding MGCM-MTGCM simulated outputs: (a) latitudinal mean density variations, (b) longitude mean density variations, and (c) diurnal variations. These specific comparisons are useful for model validation, and as will be shown the comparisons offer confidence that model results can provide predictive capability for MRO aerobraking.

Results

MGS2 simulated density variations

Table 1 includes zonal mean 120 km densities within each of the five latitude bins of interest from both MGS2 aerobraking accelerometer measurements and the corresponding MGCM-MTGCM simulated densities for the Mars conditions outlined in the previous section. Latitudinal density variations from both observations and simulation exhibit declining density values from the local Spring to Winter hemispheres, in accord with the variation of solar insolation. In particular, observed and simulated densities are both shown to decrease from the equator to the South pole by a

factor of 2.5-3.0. However, MGCM-MTGCM mean densities are slightly smaller than observed in each latitude bin, by ~20-30%. Figure 1 illustrates this same latitudinal comparison of observed and modeled MGS2 densities. MGCM-MTGCM calculated densities are presented with vertical "error" bars corresponding to the range of longitudinal density variations. It is clear that the simulations underestimate the observed MGS2 mean densities by ~20-30%. However, the observed MGS2 latitudinal and diurnal trends are reasonably reproduced by these MGCM-MTGCM simulations.

Simulated density maps at 120 km for several constant solar local time (SLT) conditions are shown in Figure 2. These maps correspond to MGS spacecraft sampling at nearly constant SLT conditions for multiple aeropasses spanning a wide range of longitudes. Longitudinal density variations are observed to change as SLT conditions are advanced. A prominent wave-3 pattern is observed over 30N-60N (SLT = 1600), with an amplitude that is ~30% of the mean density (~9.5 kg/km³). The equatorial region (SLT=1600) densities reveal a mixed wave 2 and 3 pattern with a combined amplitude that is ~25-33% of the mean (~4.2 kg/km³). The longitude phasing in this equatorial region is similar to that at northern mid-latitudes. These equatorial wave 2 and 3 patterns and amplitudes are in good accord with MGS2 accelerometer observations (e.g. Withers et al. 2003).

At mid-southern latitudes (SLT=1500), a prominent wave-2 pattern is present with an amplitude that is 25-40% of the mean (~2.8 kg/km³). MGS2 data tidal analysis shows a mixed wave-2 and 3 pattern, with combined amplitudes up to ~40% (Withers et al. 2003). Finally, at high southern latitudes (60S-90S) on both the dayside and nightside, prominent wave-1 plus weak wave-2 longitude variations are simulated, with combined amplitudes that are ~20-30% of the mean density values (2.6 kg/km³ dayside, 1.7 kg/km³ nightside). It is noteworthy that the phasing of these simulated wave-1 oscillations shifts ~30-60° westward from the dayside (SLT=1500) to the nightside (SLT=0200). Overall, the coupled MGCM-MTGCM simulations yield somewhat small wave amplitudes at high southern latitudes (winter polar region) compared to MGS2 accelerometer densities. In addition, wave-2 features are observed but wave-1 oscillations are simulated in this southern polar night region.

Table 3. MGS Phase 2 Fractional Tidal Amplitudes from MGCM-MTGCM Simulation at 120 km ($L_S = 90$).

Tidal Mode (σ, s)	0°S Latitude	30°S Latitude	60°S Latitude	75°S Latitude
(1,1)	0.07	0.04	0.14	0.13
(1,-1)	0.08	0.08	0.03	0.10
(1,-2)	0.05	0.12	0.04	0.01
(2,2)	0.05	0.05	0.06	0.02
(2,-1)	0.03	0.02	0.01	0.06

Fractional amplitudes (\pm from mean) are calculated with respect to the zonal mean density at the given latitude and altitude.

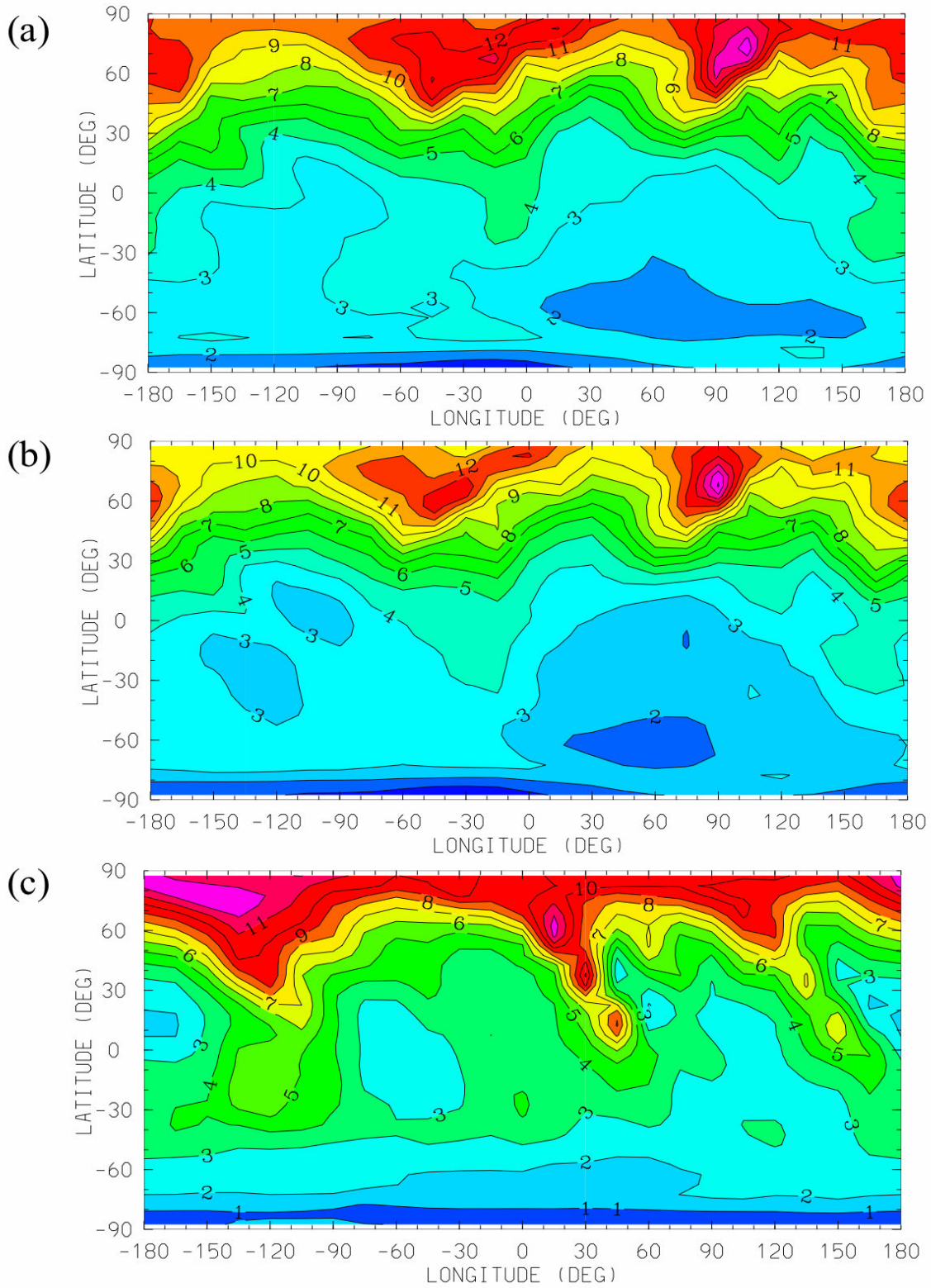


Figure 2. MGCM-MTGCM simulation for MGS2 conditions. Densities are illustrated on latitude versus longitude slices at 120 km for constant solar local time (SLT) conditions: (s) SLT = 1600; (b) SLT = 1500; and (c) SLT = 0200. Density units are kg/km³. ([figure2.pdf](#))

Previous studies have suggested that non-migrating thermal tidal mode forcing is responsible for longitudinal thermospheric wave features observed during MGS2 (Forbes and Hagan 2000; Forbes et al. 2002; Wilson 2002; Withers et al. 2003; Angelats-i-coll et al. 2004). Are the simulated harmonics (at constant SLT) illustrated in Figure 2 due to diurnal or semi-diurnal tidal modes that are eastward or westward propagating?

Table 3 summarizes results from a frequency-wave number decomposition of simulated 120 km densities for the MGS2 MGCM-MTGCM case. Fractional amplitudes are tabulated for each of five tidal modes, which are delineated by frequency (σ) and wavenumber (s) indices. Diurnal ($\sigma=1$) and semidiurnal ($\sigma=2$) tidal modes having various wavenumbers ($s = -2, -1, 1, 2$) are identified. Non-migrating (eastward propagating) tidal modes correspond to those with negative wave numbers. Equatorial region wave 2 and 3 features appear to be driven by (1,-1) and (1,-2) tidal mode forcing. This is consistent with the Diurnal Kelvin waves 1 and 2 identified in the MGS2 tidal analysis by Withers et al. (2003). At mid-southern latitudes (30-60S), the simulated prominent wave 2 pattern may also be influenced by a wave 3 component, since both (1,-1) and (1,-2) tidal modes also contribute significantly in this region. Finally, at high southern latitudes (60-90S), prominent wave 1 and weak wave-2 features are visible in Figure 2. However, tidal decomposition clearly shows (1,-1) forcing is dominant, which is expected to produce a wave 2 feature.

In summary, MGCM-MTGCM simulations generally reproduce the observed MGS2 latitudinal and diurnal trends in densities. However, it is clear that these simulations underestimate the observed MGS2 mean densities by ~20-30%. Observed longitudinal density variations are well matched by these simulations at mid-to-equatorial latitudes. However, in the high southern latitudes (corresponding to the winter polar night), simulated longitude variations are somewhat weaker and structurally different than observed.

MRO predicted density variations

Table 4 presents values of the MGCM-MTGCM predicted 120 km zonal mean densities within L_s and latitude bins corresponding to the anticipated MRO aerobraking conditions. The best comparison between MGS2 and MRO densities occurs at $L_s = 85-90$ conditions near the South pole. Simulated MRO conditions indicate that 120 km densities decline from 70S-90S into the polar night. In particular, 120 km zonal mean densities are shown to decrease by ~35% over this latitude range, while increasing by a factor of ~2.5-5.0 toward equatorial latitudes on the nightside. Predicted MRO densities near the South pole ($\leq 1.4 \text{ kg/km}^3$) are less than both simulated and observed MGS2 values. This reduction may be the result of a somewhat weaker thermospheric circulation (owing to reduced solar EUV heating) during a different phase ($F10.7 = 100$) of the solar cycle than MRO will experience.

Figure 3 illustrates latitudinal variations of predicted MRO densities. These MGCM-MTGCM calculated densities are

Table 4. MRO Predicted Latitudinal Density Variations at 120 km.

L_s	Latitude	SLT (hours)	MTGCM Zonal Mean Density (kg/km^3)
25-60	70S-80S	20-19.0	2.5
60-80	Over pole	changing	0.8-1.4
80-90	80S-60S	3.0	1.6
90-100	60S-20S	3.0	3.2
100-109	20S-20N	3.0	4.0

¹Density units (kg/km^3) are those used in aerobraking operations. These units can be translated to kg/m^3 by multiplying by 1.0×10^{-9} .

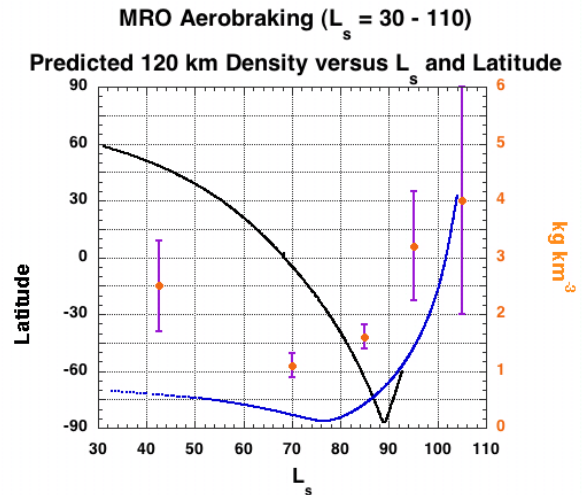


Figure 3. MRO aerobraking predicted densities at 120 km as a function of latitude. The blue curve tracks the MRO periapsis latitude variation as a function of L_s . The black curve similarly tracks the MGS2 latitude variation. Overlap occurs near $L_s = 85-95$. MRO predicted densities (L_s and latitude variations) are also found in Table 4. Density units are kg/km^3 . ([figure3.jpg](#))

presented with vertical “error” bars corresponding to the simulated range of longitudinal density variations. Again, it is clear that the MRO predicted 120 km densities are smaller than corresponding observed and simulated 120 km densities from the MGS2 database (see Figure 1). Solar local time differences between MGS2 and MRO sampling certainly contribute to these differences.

Simulated density maps at 120 km for constant SLT conditions are presented in Figure 4. These maps correspond to anticipated MRO conditions (dust load, F10.7 flux) and spacecraft sampling at nearly constant SLT conditions for a wide range of longitudes. Longitudinal density variations are again predicted to change as SLT conditions are advanced.

On the dayside (SLT = 2000-1900) at high southern latitudes, moderate wave-1 longitude variations are simulated, with amplitudes that are ~33% of the mean ($\sim 2.5 \text{ kg/km}^3$). Conversely, on the nightside (SLT = 0300), these moderate wave-1 variations (~20-30%) at high southern latitudes give way to a strong wave-2 pattern which grows in importance over 60-20S latitude. Wave-2 amplitudes are calculated to

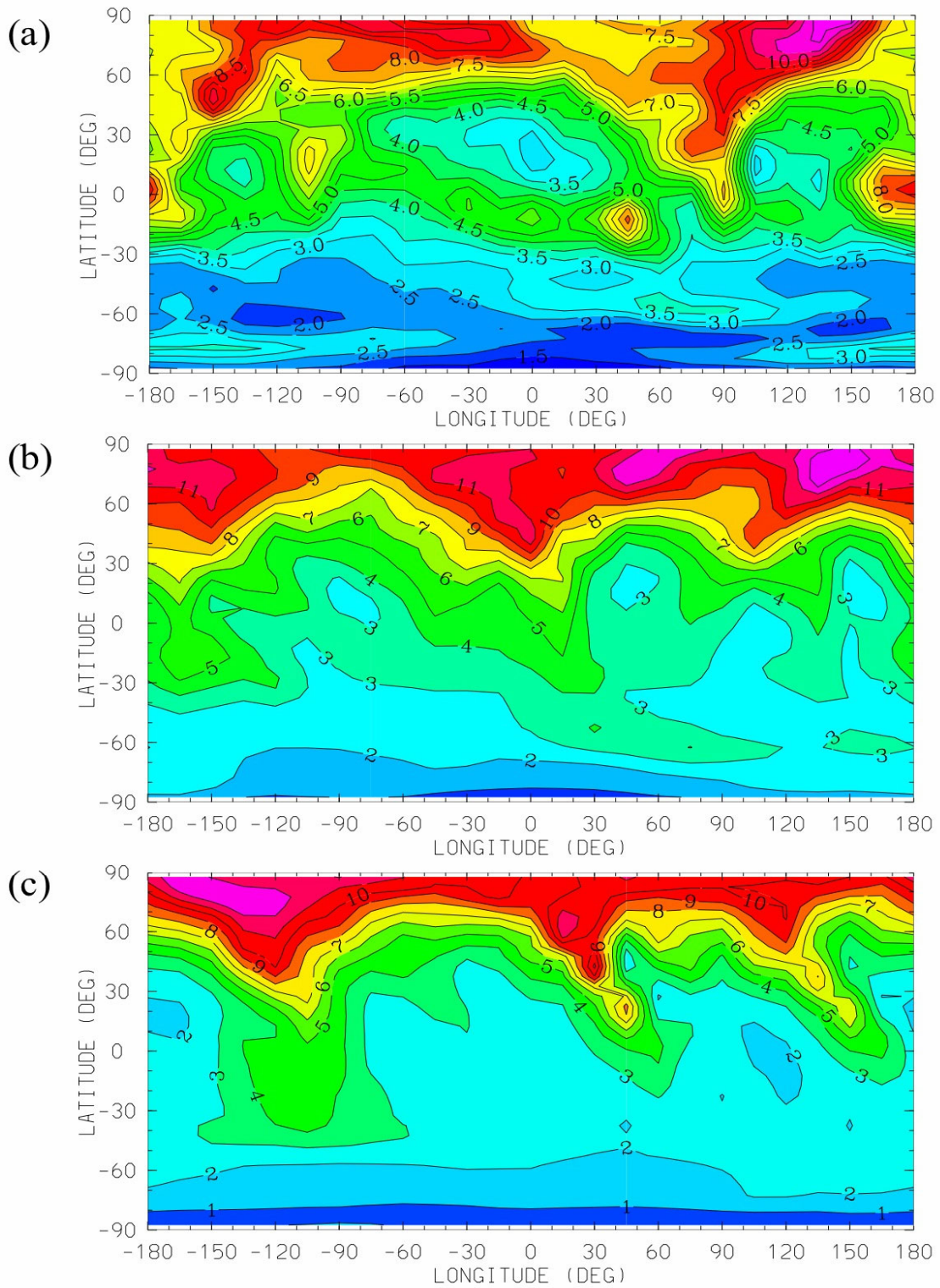


Figure 4. MGCM-MTGCM simulation for MRO conditions. Density (kg/km³) slices at 120 km: (a) SLT = 2000; (b) SLT = 1900; and (c) SLpT = 0300. ([figure4.pdf](#))

reach ~40% of the mean densities (1.6 kg/km^3 to 3.2 kg/km^3) (see Table 4). Near the equator (20S-20N), a strong wave-3 pattern is predicted with an amplitude that is up to ~50% of the mean density ($\sim 4.0 \text{ kg/km}^3$). Sampling at nightside equatorial latitudes has not been conducted thus far at this season ($L_S \sim 90$). The confirmation of such a strong wave-3 tidal signature with new MRO accelerometer measurements would be a key validation of the coupled MGCM-MTGCM simulations. These wave-3 tidal features appear in both nightside (SLT = 0200-0300) MGS2 and MRO simulations at equatorial to northern hemisphere latitudes, with the same longitudinal tidal phasing. Density peaks appear at these longitudes: 0-45E, 90-130E, and 200-260E.

Table 5 summarizes results from a frequency-wave number decomposition of simulated 120 km densities for the MRO MGCM-MTGCM case ($L_S = 90$). Similar tidal forcing features are reproduced here as indicated previously for MGS2 simulations in Table 3.

Table 5. MRO Fractional Tidal Amplitudes from MGCM-MTGCM Simulation at 120 km ($L_S = 90$).

Tidal Mode (σ, s)	0°S Latitude	30°S Latitude	60°S Latitude	75°S Latitude
(1,1)	0.06	0.04	0.13	0.15
(1,-1)	0.09	0.08	0.03	0.11
(1,-2)	0.05	0.13	0.04	0.02
(2,2)	0.05	0.055	0.05	0.02
(2,-1)	0.03	0.02	0.01	0.06

Fractional amplitudes (\pm from mean) are calculated with respect to the zonal mean density at the given latitude and altitude.

In summary, predicted MRO aerobraking 120 km densities are slightly smaller than corresponding densities from MGS2 simulations with overlapping latitude coverage. This is likely due to: (a) different SLT sampling at a given latitude, and (b) a weaker thermospheric circulation resulting from expected solar minimum (MRO) versus solar moderate (MGS2) conditions. However, the latitudinal and diurnal density trends should be similar for the two observing periods. On the nightside, at mid-to-equatorial latitudes, wave-2 and 3 oscillations should be quite significant during MRO aerobraking. These wave patterns should be considered when conducting MRO aerobraking exercises.

Conclusions

It is important to reliably predict the structure of the Mars lower thermosphere for the benefit of upcoming MRO aerobraking exercises. Previous MGS accelerometer measurements during Phase 2 (MGS2) of aerobraking were obtained during similar martian seasons ($L_S \sim 30-95$) at southern latitudes as will be the MRO accelerometer measurements. However, the solar local time versus latitude coverage for a given period during this season is generally different for the two spacecraft. Therefore, coupled MGCM-MTGCM model simulations are first validated using MGS accelerometer data, and then utilized to predict martian lower thermosphere structure for conditions expected during MRO aerobraking exercises. In particular, observed MGS2 120 km

density data are compared with corresponding MGCM-MTGCM simulated outputs: (a) latitudinal mean density variations, (b) longitude mean density variations, and (c) diurnal variations. These specific comparisons are crucial for model validation, before proceeding to thermospheric predictions for the MRO aerobraking period.

MGCM-MTGCM simulations generally reproduce the observed MGS2 latitudinal and diurnal trends in densities. However, it is clear that these simulations underestimate the observed MGS2 density magnitudes by ~20-30%. Observed longitudinal density variations are well matched by these simulations at near-equatorial and northern hemisphere latitudes. However, in the high southern latitudes (corresponding to the winter polar night), simulated longitude variations are somewhat weaker than observed. These comparisons suggest that the coupled MGCM-MTGCM simulations capture most of the behavior of the Mars lower thermosphere at this season for these latitudes and solar local times. The overall discrepancy between calculated and observed zonal mean density magnitudes may reflect slightly warmer actual temperatures at lower altitudes (below 100 km) in the winter polar night than are being simulated. Longitudinal density variations at high southern latitudes may also be under-estimated, for reasons not yet identified. This suggests that reliable predictions of the Mars lower thermospheric structure at high southern latitudes may be somewhat problematic. However, MGCM-MTGCM predictions of mid-to-equatorial latitude mean densities, and their longitude variations, should be more reliable.

In general, MRO predictions of thermospheric properties at 120 km reveal decreasing dayside densities from 70S to 90S. Simulated density values then decrease as the periapsis migrates to the nightside at high southern latitudes. Subsequently, these nightside density values increase by a factor of 2.5-5 as periapsis latitude migrates to and beyond the equator. This behavior is consistent with a cold winter polar atmosphere which becomes warmer on the nightside. This nightside warming and density increase result from a strong inter-hemispheric circulation which yields dynamical (adiabatic) heating and horizontal advection impacting the nightside (Bougher et al. 2006). Longitude density variations are predicted to be moderate (20-30% of the mean) at high southern latitudes, before increasing to 30-50% of the mean at mid-to-equatorial latitudes on the nightside. Wave-2 and 3 longitudinal density variations should be significant on the deep nightside, and worthy of consideration for aerobraking planning. Our MRO predicted density uncertainties are constructed from summing the: (a) underestimated longitude variations for high southern latitude bins, and (b) the overall underestimate of zonal mean densities gleaned from MGS2 comparisons. MRO predictions are thus deemed to be most reliable in the 20N to 60S latitude region (~20-30% uncertainty), and less reliable in the 60S-90S latitude region ($\leq 50\%$ uncertainty).

We emphasize that these MRO predictions are based upon MGCM-MTGCM model simulations, which are only as good as estimated inputs for solar flux conditions and Mars dust

opacity distributions. We make no guarantees. However, these MRO predictions should serve as a guide for aerobraking planning and daily aerobraking advisory. We look forward to new MRO accelerometer measurements in order to continue our model validation studies, and to further the characterization of the martian upper atmosphere.

Directory of Supporting Data

[root directory](#)

[manuscript.pdf](#)

Fig. 1 [figure1.jpg](#) full resolution graphic

Fig. 2 [figure2.pdf](#) full resolution graphic;
[figure2.txt](#) simulation data in tabular form

Fig. 3 [figure3.jpg](#) full resolution graphic

Fig. 4 [figure4.pdf](#) full resolution graphic;
[figure4.txt](#) simulation data in tabular form

Table 2 [modelinputs.txt](#) MGCM-MTGCM input parameters for simulations

Acknowledgements

We wish to thank M. A. Lopez-Valverde for the CO₂ NLTE 15-micron cooling subroutine used in all these MGCM-MTGCM calculations. The MRO latitude versus L_5 estimate is provided by Robert Tolson. This research was supported in part by the NASA Mars Data Analysis Program, and the Mars Reconnaissance Orbiter Project Office. Bougher was specifically supported by grant NNG04GJ94G from NASA and 1277433 from JPL. Murphy was supported by grants NAG5-12123 from NASA and 1282764 from JPL. The MGS data are available from the PDS Atmospheres Node.

References

- Angelats-i-Coll, M., et al. (2004) "Upper atmosphere of Mars up to 120 km: Mars Global Surveyor accelerometer data analysis with the LMD general circulation model" *Journal of Geophysical Research*, 109, E01011. [doi:10.1029/2003JE002163](#)
- Angelats-i-Coll, M., F. Forget, M. A. Lopez-Valverde, and F. Gonzalez-Galindo (2005) "The first Mars thermospheric general circulation model: The Martian atmosphere from the ground to 240 km" *Geophysical Research Letters*, 32, L04201. [doi:10.1029/2004GL021368](#)
- Banfield, D. B. Conrath, J.C. Pearl, M.D. Smith, and P. Christensen (2000) "Thermal tides and stationary waves on Mars as revealed by Mars Global Surveyor thermal emission spectrometer" *Journal Geophysical Research-Planets*, 105, 9521-9537.
- Banfield, D., B.J. Conrath, M.D. Smith, P.R. Christensen, and R.J. Wilson (2003) "Forced waves in the martian atmosphere from MGS TES nadir data" *Icarus* 161, 319-345.
- Bridger, A.F.C., and J.R. Murphy (1998) "Mars' surface pressure tides and their behavior during global dust storms" *Journal of Geophysical Research-Planets* 8587-8601.
- Bougher, S. W., S. Engel, R. G. Roble, and B. Foster (1999) "Comparative terrestrial planet thermospheres: 2. Solar cycle variation of global structure and winds at equinox" *Journal of Geophysical Research* 104, 16, 591-16, 611.
- Bougher, S. W., et al. (1999) "Mars Global Surveyor aerobraking: Atmospheric trends and model interpretation" *Advances in Space Research* 23, 1887-1897.
- Bougher, S. W., S. Engel, R. G. Roble, and B. Foster (2000) "Comparative terrestrial planet thermospheres: 3. Solar cycle variation of global structure and winds at solstices" *Journal of Geophysical Research* 105, 17669-17692.
- Bougher, S. W., S. Engel, D. P. Hinson, and J. R. Murphy (2004) "MGS Radio Science Electron Density Profiles : Interannual variability and implications for the neutral atmosphere" *Journal of Geophysical Research* 109, E03010. [doi:10.1029/2003JE002154](#)
- Bougher, S. W., J. M. Bell, J. R. Murphy, M. A. Lopez-Valverde, and P. G. Withers (2006) "Polar warming in the Mars thermosphere: Seasonal variations owing to changing insolation and dust distributions" *Geophysical Research Letters* 32, L02203. [doi:10.1029/2005GL024059](#)
- Bougher, S. W., J. M. Bell, J. R. Murphy, and R. Lillis (2006) "Inter-annual variability of the Mars thermosphere: New simulations and comparison with recent Mars datasets" *Proceedings of the Granada Mars Atmospheric Modeling Workshop, Granada, Spain, 27-February to 3-March*.
- Conrath, B. J. (1975) "Thermal structure of the Martian atmosphere during the dissipation of the dust storms of 1971" *Icarus* 24, 36-46.
- Forbes, J. M. and M. Hagan (2000) "Diurnal Kelvin wave in the atmosphere of Mars: Towards an understanding of "stationary" density structures observed by the MGS accelerometer" *Geophysical Research Letters* 27, 3563-3566.
- Forbes, J. M., et al. (2002) "Nonmigrating Tides in the Thermosphere of Mars" *Journal of Geophysical Research* 107 (E11) 5113. [doi:10.1029/2001JE001582](#)
- Gonzalez-Galindo, F., M. A. Lopez-Valverde, M. Angelats-i-coll, and F. Forget (2005) "Extension of a Martian general circulation model to thermospheric altitudes: UV heating and photochemical models" *Journal of Geophysical Research* 110, E09008. [doi:10.1029/2004JE002312](#)
- Haberle, R. M., et al. (1999) "General Circulation Model Simulations of the Mars Pathfinder Atmospheric Structure Investigation/Meteorology Data" *Journal of Geophysical Research* 104, 8957-8974.
- Keating, G. M. and N. C. Hsu (1993) "The Venus atmospheric response to solar cycle variations" *Geophysical Research Letters* 20, 2751-2754.
- Keating, G. M. et al. (1998) "The structure of the upper atmosphere of Mars: In-situ Accelerometer measurements from Mars Global Surveyor" *Science* 279, 1672-1676.
- Keating, G. M., R. H. Tolson, J. L. Hanna, R. F. Beebe, J. R. Murphy, and L. Huber (2001) "MGS-M-ACCEL-5-ALTITUDE-V1.1" *NASA Planetary Data System, NASA Goddard Spaceflight Center, Greenbelt, MD*.
- Keating, G. M., R. H. Tolson, J. L. Hanna, R. F. Beebe, J. R. Murphy, and L. Huber (2001) "MGS-M-ACCEL-5-PROFILE-V1.1, , NASA Planetary Data System" *NASA Goddard Spaceflight Center, Greenbelt, MD*.
- Keating, G. M. et al. (2003) "Brief review on the results obtained with the MGS and Mars Odyssey 2001 Accelerometer Experiments" *Proceedings, International workshop: Mars atmosphere modeling and observations, Granada, Spain, 13-15 January*.
- Lillis, R. J., J. H. Engel, D. L. Mitchell, D. A. Brain, R. P. Lin, S. W. Bougher, and M. H. Acuna (2005) "Probing upper thermosphere neutral densities at Mars using electron reflectometry" *Geophysical Research Letters* 32, L23204. [doi:10.1029/2005GL024337](#)

- Liu, J., M. I. Richardson, and R. J. Wilson (2003) "An assessment of the global, seasonal, and inter-annual spacecraft record of Martian climate in the thermal infrared" *Journal of Geophysical Research* 108, (E8), 5089. [doi:10.1029/2002JE001921](https://doi.org/10.1029/2002JE001921)
- Smith, M. D. (2004) "Interannual variability in TES atmospheric observations of Mars during 1999-2003" *Icarus* 167, 148-165.
- Tolson, R. H., et al. (1999) "Utilization of Mars Global Surveyor Accelerometer data for atmospheric modeling" *Astrodynamics* 103, 1329-1346.
- Tolson, R. H., et al. (2005) "Application of Accelerometer data to Mars Odyssey aerobraking and atmospheric modeling" *Journal of Spacecraft and Rockets* 42, 435-443.
- Wilson, R.J., and K. Hamilton (1996) "Comprehensive model simulation of thermal tides in the Martian atmosphere" *Journal of the Atmospheric Sciences* 53, 1290-1326.
- Wilson, R.J. (2000) "Evidence for diurnal period Kelvin waves in the Martian atmosphere from Mars Global Surveyor TES data" *Geophysical Research Letters* 27, 3889-3892.
- Wilson, R. J. (2002) "Evidence for nonmigrating thermal tides in the Mars upper atmosphere from the Mars Global Surveyor Accelerometer Experiment" *Geophysical Research Letters* 29(7) 1120. [doi:10.1029/2001GL013975](https://doi.org/10.1029/2001GL013975)
- Withers, P. G., S. W. Bougher, and G. M. Keating (2003) "The effects of topographically controlled thermal tides in the Martian upper atmosphere as seen by the MGS Accelerometer" *Icarus* 164, 14-32.
- Withers, P. G. (2006) "Mars Global Surveyor and Mars Odyssey Accelerometer observations of the Martian upper atmosphere during aerobraking" *Geophysical Research Letters* 33, L02201. [doi:10.1029/2005GL024447](https://doi.org/10.1029/2005GL024447)